

RESEARCH ARTICLE | MAY 17 2024

The impact of alcohol and ammonium fluoride on pressure-induced amorphization of cubic structure I clathrate hydrates

Special Collection: [Porous Solids for Energy Applications](#)

Lilli-Ruth Fidler ; Paul Posch ; Johannes Klocker ; Thomas S. Hofer ; Thomas Loerting  



J. Chem. Phys. 160, 194504 (2024)

<https://doi.org/10.1063/5.0203916>

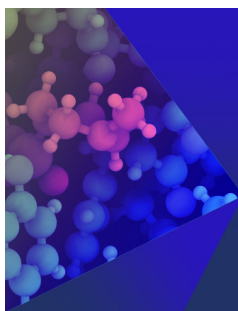


View
Online



Export
Citation

12 July 2024 18:31:29



The Journal of Chemical Physics

Special Topic: Molecular Dynamics, Methods
and Applications 60 Years after Rahman

Submit Today



The impact of alcohol and ammonium fluoride on pressure-induced amorphization of cubic structure I clathrate hydrates

Cite as: J. Chem. Phys. 160, 194504 (2024); doi: 10.1063/5.0203916

Submitted: 17 February 2024 • Accepted: 28 April 2024 •

Published Online: 17 May 2024



View Online



Export Citation



CrossMark

Lilli-Ruth Fidler,¹  Paul Posch,¹  Johannes Klocker,²  Thomas S. Hofer,²  and Thomas Loerting^{1,a)} 

AFFILIATIONS

¹Institute of Physical Chemistry, University of Innsbruck, Innrain 52c, A-6020 Innsbruck, Austria

²Institute of General, Inorganic and Theoretical Chemistry, University of Innsbruck, Innrain 80, A-6020 Innsbruck, Austria

Note: This paper is part of the JCP Special Topic on Porous Solids for Energy Applications: Clathrate Hydrates, Metal-Organic Frameworks (MOF), and Covalent-Organic Frameworks (COF)

^{a)}Author to whom correspondence should be addressed: thomas.loerting@uibk.ac.at

ABSTRACT

We have investigated pressure-induced amorphization (PIA) of an alcohol clathrate hydrate (CH) of cubic structure type I (sI) in the presence of NH₄F utilizing dilatometry and x-ray powder diffraction. PIA occurs at 0.98 GPa at 77 K, which is at a much lower pressure than for other CHs of the same structure type. The amorphized CH also shows remarkable resistance against crystallization upon decompression. While amorphized sI CHs could not be recovered previously at all, this is possible in the present case. By contrast to other CHs, the recovery of the amorphized CHs to ambient pressure does not even require a high-pressure annealing step, where recovery without any loss of amorphicity is possible at 120 K and below. Furthermore, PIA is accessible upon compression at unusually high temperatures of up to 140 K, where it reaches the highest degree of amorphicity. Molecular dynamics simulations confirm that polar alcoholic guests, as opposed to non-polar guests, induce cage deformation at lower pressure. The substitution of NH₄F into the host-lattice stabilizes the collapsed state more than the crystalline state, thereby enhancing the collapse kinetics and lowering the pressure of collapse.

© 2024 Author(s). All article content, except where otherwise noted, is licensed under a Creative Commons Attribution (CC BY) license (<https://creativecommons.org/licenses/by/4.0/>). <https://doi.org/10.1063/5.0203916>

I. INTRODUCTION

Clathrate hydrates are ice-like materials containing pores of a few Ångström. They are similar to zeolites, which are used as molecular sieves. At low temperature and/or high pressure, water forms geometric, cage-like, and space-filling cavities around its gaseous guest. In fact, clathrate hydrates (CHs) are able to store more than 160 gas volumes per hydrate volume.¹ With this versatile ability to store large amounts of gases, CHs are becoming more and more relevant in energy applications.² Hydrate-based gas separation offers the possibility of the purification of natural gases.³ CHs could also be used for the storage and transportation of fuels, such as methane or hydrogen,⁴ so that they are studied as an alternative to conventional fossil fuels.^{5,6} Natural methane hydrate deposits exist in abundance in marine and Arctic sediments.⁷ These reserves of methane are estimated to surpass those of other fossil fuels by about ten times.⁸

Undoubtedly, CHs will play a role in challenges in energy applications, but the kinetics and thermodynamics of their formation and decomposition are still far from being fully understood, so many open questions need to be tackled. For once, the pressure of formation needs to be lowered for cost-effective application. In addition, growth and dissociation kinetics need to be enhanced to be technologically relevant.⁹ The most promising way to get started is by studying promoters and inhibitors of CH formation. Interestingly, while these two roles appear to be opposites, methanol takes both.

Typically, CHs form in the presence of hydrophobic guests, e.g., noble gases, methane, or tetrahydrofuran (THF), under cryo-conditions and/or pressure. These guests are then engaged in an H₂O framework and interact hydrophobically with the hydrate lattice, stabilizing the guest-host structure through van der Waals repulsion. The size of the guest determines cage size, which then leads to distinct structure types. Smaller guests, e.g., methane, form

cubic structure I (sI) CHs. The sI CH consists of six large (T, $5^{12}6^2$) and two small cages (D, 5^{12}) per unit cell. Larger guests, e.g., THF, induce the formation of cubic structure II (sII) for their larger cages (H, $5^{12}6^4$). Eight H cages form the sII unit cell, together with 16 small D cages. Hydrophilic guest molecules, such as methanol, usually form hydrogen bonds with the framework itself and cause destabilization. For this reason, methanol is considered an effective thermodynamic inhibitor of hydrate formation and is commonly used in the gas and oil industries for the prevention of hydrate plug formation.¹⁰ The formation of alcohol CHs is, however, not entirely impossible. For implementation into the host framework, the addition of hydrophobic helper guest molecules, such as methane,^{11–15} THF,^{16,17} carbon dioxide,¹⁸ ethylene oxide,¹⁷ or acetylene,¹⁸ is required. Methanol has even been shown to be a kinetic promoter of hydrate formation. Frozen water that has been doped with methanol shows an accelerated hydrate formation during exposure to gaseous guests such as methane,^{19,20} propane,²¹ or carbon dioxide.²⁰ Though the exact mechanism is not fully understood, it has been suggested that methanol causes vacancies on the ice lattice,^{19,21} either Bjerrum L-defects²² or guest-stabilizing defects and interstitials.²³ These vacancies enhance guest molecule diffusion and consequently increase the formation rate. Similarly, methanol also promotes hydrate formation when made *via* vapor-co-deposition at temperatures below 150 K instead of freezing from the aqueous solution.^{16,18} That is, methanol's ability to inhibit hydrate formation is limited to its synthesis directly from aqueous solutions.

Shin *et al.*^{24,25} have made advances in the synthesis of methanol CHs from aqueous solutions, eliminating the requirement for a hydrophobic helper guest molecule. Instead, they tune the properties of the host network by substituting some of the water molecules. Specifically, they added up to 27 mol. % of ammonium fluoride (NH_4F), which is known to form ice-like phases on its own and solid solution frameworks with water.^{26,27} Due to their isoelectronic and isostructural properties, NH_4^+ and F^- are incorporated into the crystal structure by replacing two water molecules. That is, clathrates of cubic structure type I, II (sI and sII, respectively) and hexagonal structure type H (sH) can be synthesized with methanol and other alcohols as guest molecules after replacing some water molecules with NH_4F . The size of the alcohol molecules determines the structure type; e.g., ethanol and methanol result in sI,²⁵ while methanol and THF lead to a sII CH.²⁸ A number of NH_4F -containing CHs have been synthesized since the seminal work.^{24,25,28–31} None of these unusual CHs have so far been studied at elevated pressure, though. For this reason, our main focus is on assessing the high-pressure behavior of NH_4F -alcohol CHs. Under pressure, both guest and host molecules are forced closer to each other, allowing for pressure-induced transformations. The nature of such transformations could help reveal more about guest–host interactions.

In contrast to the situation for NH_4F -containing CHs, the phase behavior of pure- H_2O sI and sII CHs upon pressurization has been extensively studied.^{32–50} Just like pure H_2O hexagonal ice (I_h)⁵¹ (without any guest molecules), CHs undergo pressure-induced amorphization (PIA) at low temperatures of up to 135–140 K.^{33,52} The PIA of I_h was first observed in 1984 by Mishima upon compression at 77 K to 1.0 GPa.⁵¹ In the low temperature region (77–130 K), ice I transforms into unannealed high-density amorphous (uHDA)

ice. This HDA-subtype contains distorted, crystalline remnants.^{53–55} Temperature-annealing then leads to a transformation into one of the three equilibrated forms of amorphous ice. Low-density amorphous ice (LDA) forms in the pressure range below 0.2 GPa,⁵⁶ while between 0.2 and 0.8 GPa expanded high-density amorphous (eHDA) ice⁵⁷ and above 0.8 GPa very high-density amorphous (VHDA) ice form.⁵⁸ PIA is frequently interpreted as the crossing of the extended negatively sloped melting line into the low-temperature range,^{51,59} which in itself is considered an anomalous property of ice.

Similar to pure ice I_h , sI and sII CHs exhibit negatively sloped melting lines, while sH CHs do not.⁶⁰ Consequently, sH CHs do not experience PIA, while sI and sII CHs do. For CHs, PIA was first observed for a sII CH in 1982 by Ross and Andersson,⁴³ though at this point its amorphous nature was unknown. The link to the PIA of I_h was made in 1986 by Johari and Jones,⁴⁶ who interpreted amorphization as a mechanical collapse of the polycrystalline clathrate. Since then, PIA has been observed for sII THF,^{32–35,42–50} sII SF_6 ,³² sII Ne,³⁶ sII Ar,^{37,38} and even larger organic guest molecules like acetone,⁴² 1-3-dioxolane,^{33,34,42} and cyclobutanone.^{33,35,42} Amorphization pressures range from 0.8 to 1.6 GPa at temperatures between 77 and 135 K, as compared to 1.0 GPa for I_h .⁵¹

PIA of sI clathrates has been observed as well, namely for xenon,³⁷ methane,^{39–41} and ethane hydrates,⁴¹ though at significantly higher pressures. Xe hydrates remain crystalline at pressures of at least 4 GPa,³⁷ and methane hydrates undergo PIA at 3.2 GPa and 100 K.^{39–41} Ethane hydrates begin to amorphize at 4 GPa, 100 K.⁴¹ Similarly, PIA has also been observed for the silica analogs of CHs, clathrasils,⁶¹ *i.e.*, PIA is not restricted to CHs with pure water frameworks. Yet, PIA or even compression of any alcohol-containing CH has not been studied previously, and so it is the focus of the present work.

The first question is, of course, whether or not PIA takes place in such clathrates. If so, secondary questions are at which pressure, whether the amorphized CH remains amorphous even after releasing the pressure, or whether it reverts back to the crystalline clathrate. In the case of pure water without guests, amorphous ice can be recovered at 77 K but reverts to crystalline ice at higher temperatures, typically above 140 K.⁶² This is different in the case of amorphized CHs. They typically cannot be recovered even at 77 K. Upon decompression, most CHs revert to crystallinity.³² An early computational study on sI noble gas hydrates has predicted that crystallization of amorphized CHs can only be prevented at 0 K.⁶³ At any finite temperature, nucleation of the cage structure around the guest molecules induces crystallization upon decompression.⁶³ This begs the question of whether the hydrophobic character of the guests is responsible for preserving some structure even between the amorphized water molecules, ready to retain their crystallinity at lower pressures.

In spite of these computational results,⁶³ ways around crystallization upon decompression were realized in experiments, making amorphized clathrates available at ambient pressure. Suzuki *et al.* used annealing at 1.5 GPa and above and at 150 K and above to recover amorphous (RA) clathrates to ambient pressure.^{44,45} The key to this success seems to be a transformation to the more dense very-high-density-amorphous-like (VHDA) clathrate at ≥ 1.5 GPa/ ≥ 150 K. Rapid cooling of the VHDA-like clathrate, followed by decompression, results in the recovery of

amorphous (RA) clathrate of a lower density, which turns out to be in-between the LDA-like and HDA-like CH.^{38,42} These polyamorphs can only be distinguished *in situ*, which has been performed so far for amorphized sII Ar³⁸ and THF clathrates.^{42,48} It has been suggested that annealing at high pressure eliminates nucleation sites and, therefore, makes some amorphous clathrates resistant to crystallization and recoverable at low temperatures.⁴² The crystallization of RA then takes place at ambient pressures above 120 K.^{37,38,48} Though a recoverable amorphous CH phase has been observed with Ar^{37,38} and THF hydrates⁴⁸ (sII), Xe hydrates³⁷ (sI) always revert back to crystallinity upon decompression at low temperatures, even after annealing at high pressures. Annealing methane hydrate (sI) at high pressures does not result in a transformation to an amorphous CH, but instead, the amorphous CH crystallizes into a denser, crystalline methane hydrate structure (MH-III).⁵⁴ Thus far, sI CHs cannot be recovered to ambient pressure at all. It is unclear how alcohol molecules act as guests in the cavities of sI CHs and how NH₄F–H₂O host networks affect this behavior, and so this is our focus here.

That is, we here investigate the phase behavior of an ethanol + methanol CH of sI type with an H₂O–NH₄F host structure. Rather than the typical hydrophobic guest, we use a guest that is partly hydrophilic and has the ability to hydrogen-bond with the ice cages. The guest molecules ethanol and methanol occupy the large (T) and small (D) cages, respectively. The following open questions have motivated our study: (1) Does this unusual, hydrophilic CH undergo PIA at low temperatures? (2) Does the CH experience pressure behavior similar to that of CHs with hydrophobic guests? (3) How does temperature affect the pressure-induced transformation? (4) Can an amorphous sI clathrate be recovered to ambient pressure so that *ex situ* characterization methods like x-ray diffraction can be employed to study structure, dynamics, etc.? (5) How do polar guest molecules, such as ethanol and methanol, and NH₄F incorporation into the host structure affect the behavior under pressure?

We address these questions by utilizing *in situ* dilatometry to track any pressure-induced changes, *ex situ* x-ray diffraction for sample characterization, and molecular dynamics (MD) to run multiple combinations of altered guest and host compositions.

II. METHODS

A. Sample preparation

The crystalline sI CH was prepared by mixing aqueous NH₄F and an aqueous ethanol/methanol solution. The ideal sI composition contains 46 water molecules in the host lattice, which features six large cages (T, 5¹²6²) and two small cages (D, 5¹²). We here use a 27 wt. % NH₄F solution, so that the host network is composed of 26.44 H₂O molecules and 9.78·NH₄F molecules, i.e., 19.56 water molecules are replaced by 9.78 NH₄F molecules. We mix this with a substoichiometric amount of ethanol/methanol, namely 4.72 molecules of CH₃CH₂OH and 1.57 molecules of CH₃OH filling the cages. Relating to an ideal composition of exactly one ethanol per large cage (T) and one methanol per small cage (D), the mixing ratio in this study corresponds to a 79% cage occupation of ethanol (T) and a 79% cage occupation of methanol (D). Between 400 and 600 μl of mixed liquid solutions were filled into an indium

container kept at 77 K using a microliter pipette. The whole setup was submerged in liquid nitrogen. In this procedure, cooling from ambient temperature to 77 K takes less than one minute, i.e., cooling rates are near 300 K min⁻¹. Such rates are low enough to avoid the vitrification of the solution. Instead, crystalline products freeze [see x-ray diffraction in Fig. 1(b)].

B. High-pressure dilatometric piston-cylinder experiments

For all volumetric experiments, the set-up was used that has been previously used for many years in the Loerting group.^{53,54} This set-up includes a high-pressure piston cylinder with an 8 mm bore in a commercial universal material testing machine (Zwick, model BZ100/TL3S). The sample is inside an indium container. Temperature is monitored using a Pt-100 temperature sensor and controlled using resistive heaters inserted into the piston cylinder. To reach the desired temperature, a heating rate of 3 K min⁻¹ was used.

All piston-cylinder experiments were preceded by a precompression to ~0.4 GPa and back to 0.02 GPa (0.1 GPa min⁻¹) at 77 K to squeeze out excess air and obtain smooth dilatometric curves. All samples were then compressed to 1.6 GPa (0.04 GPa min⁻¹) at different temperatures and decompressed, followed by sample recovery. To recover the sample to ambient pressure, the set-up was either rapidly cooled to 77 K with liquid nitrogen at 1.6 GPa (“high-pressure recovery”) or at 0.02 GPa (“low-pressure recovery”). Quenching rapidly to 77 K at high pressure enables the recovery of the high-pressure phase that has formed upon compression. Quenching at 0.02 GPa instead allows for the conversion of the high-pressure phase to a low-pressure phase during decompression. That is, the reversibility of pressure-induced transformations upon decompression at various temperatures can be tested.

Blind dilatometric curves were recorded to 1.6 GPa at 77 and 200 K using the same set-up but without the sample. Blind curves are used to correct the volumetric data for effects related to the compaction of the set-up itself, e.g., the compaction of steel-pistons. Interpolated blind curves were used at temperatures between 77 and 200 K. Experiments carried out at the same temperature were scaled to match the same step height of the densifying step upon compression; this normalizes the curves in cases where different initial sample volumes were used.

C. *Ex situ* x-ray diffraction

For sample characterization, powder x-ray diffraction was employed using a Siemens diffractometer, model D5000 (Cu Kα₁: λ = 0.154 18 nm, Cu Kα₂ and Cu Kβ filtered out), equipped with a low-temperature Anton Paar cryochamber. The x-ray source and the detector were employed in a θ/θ arrangement, and a Göbel-mirror was used for parallel beam optics. All measurements were carried out at 77 K in a vacuum of <1 mbar. The Loerting group has worked on avoiding ice contamination from the atmosphere during sample transfer for more than 20 years. At present, little to no hexagonal ice contamination occurs during sample loading into the diffractometer. The following measures ensure this achievement: (i) Samples are kept in liquid nitrogen at all times, except for the transfer itself. (ii) To do the transfer as quickly as possible, the clathrate samples immersed in liquid nitrogen are placed in close proximity to the

x-ray sample holder (about 10–20 cm). (iii) Samples are powdered while immersed in liquid nitrogen, where the powder is placed on a spoon, still immersed in liquid nitrogen. (iv) It takes about 3–5 s to lift the spoon out of the nitrogen, to push the powdered sample onto the sample holder, and to close the vacuum chamber. In these 3–5 s, liquid nitrogen evaporates from the sample, and as long as liquid nitrogen is evaporating from the sample, there can be no flow from the atmosphere to the sample (the flow is rather from the sample to the atmosphere!). (v) Only after 7–10 s does the evaporation of nitrogen stop, and only then condensation from humid air might take place. If the process of transfer takes longer than usual, then we put liquid nitrogen over the sample once more before the condensation starts so that again liquid nitrogen evaporates from the sample! (vi) Once there is good thermal contact between powder and sample holder (by forcing the powder onto the metal), the chamber is closed and evacuated to less than 1 mbar immediately. (vii) The chamber is always flushed with dried air, so that no water is in the chamber. The only way water is carried to the chamber is by stirring up the surrounding air through movements with the hands. This water is not given time to condense, though, and is pumped off before it can do so [see items (vi) and (iv)]. Recent examples of diffractograms for high-pressure ice phases or for amorphous ices without or with barely any hexagonal ice contamination can be found in Refs. 65–68.

D. DFTB molecular dynamics simulations

To investigate the impact of NH_4F on the structural stability of CHs, molecular dynamics (MD) simulations were carried out using a unit cell of crystalline sI CH,⁶⁹ and periodic boundary conditions were applied. Host structure and guest molecule composition were varied and combined. To realize variations in the composition of the host structure, either all 46 lattice sites were occupied with one H_2O molecule each, or 20 sites out of these were replaced with 10 pairs of $\text{NH}_4^+ \cdot \text{F}^-$. Two adjacent H_2O molecules were replaced by one NH_4F molecule manually, and their surrounding hydrogen atoms were shifted to obey the Bernal Fowler ice rules⁷⁰ again. Additionally, to cancel out any potential dipole moment deriving from the ionic character of NH_4F , two NH_4F were always placed on a hexagon of $5^{12}6^2$ cages directly across from each other, “facing” in the opposite direction. This composition corresponds to 27.8 mol. % NH_4F in a solid solution with H_2O , closely matching the 27 mol. % NH_4F in the experimental composition. In all six large (T) and two small (D) cages, exactly one guest molecule per cage was placed. Two different combinations of guest molecules were considered. In the simulation, we employed exactly six and two molecules of ethanol and methanol, respectively. This corresponds to a situation in which every single cage is filled with a single molecule, where the smaller methanol molecule fills the small cages and the larger ethanol molecule fills the larger cages. In the experiment, we also assume the occupation of every single cage with a single molecule, just like in the simulation. Yet, we cannot avoid the ice-I type by-phase in experiments, *i.e.*, there are guest-free ice-I domains in the sample and domains of clathrate hydrate that are fully filled. The overall composition of our liquid mixture would produce 79% filled cages if there was no by-phase crystallizing simultaneously. Taking the by-phase into account, $\gg 79\%$ of clathrate cages are filled, presumably even 100%. This then suggests that the onset pressures for clathrate

amorphization are mostly impacted by the chemical composition of hosts and guests. By contrast, the emptiness of cages does not play a major role here. Yet, it is known that empty cages reduce pressure-stability.³⁷ For a non-polar counterpart, six propane and two ethane molecules replace the polar alcoholic guests. Close in size, they differ primarily in polarity and interaction with the host cages.

The MD simulations were performed using self-consistent charge density functional tight binding (SCC-DFTB),^{71,72} using the DFTB + package.⁷³ The third-order implementation (DFTB3) was used in conjunction with the 3ob parameter set.^{74,75} While many MD simulations employ force fields, we here use an electronic calculation based on density functional theory. Simulations were carried out on these four systems for all possible host-guest combinations. The timestep in the velocity Verlet algorithm⁷⁶ was set to 0.5 fs. For temperature and pressure control, the Bussi-rescaling thermostat⁷⁷ ($\tau_t = 0.1$ ps) and Berendsen manostat⁷⁸ ($\tau_p = 1.0$ ps) algorithms were employed. Isotropic pressure coupling was utilized, *i.e.*, all lattice parameters of the unit cell are coupled, and the unit cell remains cubic throughout the entire simulation. The pressure was increased stepwise, from 1 atm to 0.1, 0.5, 1.0, 1.5, and finally 2.0 GPa. At each pressure, the system is simulated for a total of 20.0 ps. The associated time evolution of the applied pressure as a function of simulation time is provided in Fig. SM1 of the supplementary material.

III. RESULTS AND DISCUSSION

A. Pressure-induced amorphization: The upstroke transition

The crystalline sI ethanol + methanol clathrate hydrate (CH) with the composition of $(4.72\text{CH}_3\text{CH}_2\text{OH}; 1.57\text{CH}_3\text{OH}) \cdot (26.44\text{H}_2\text{O}; 9.78\text{NH}_4\text{F})$ was used for this study. In this stoichiometry, some cages might be empty. Our x-ray data [see Fig. 1(b), blue curve at bottom] indicate a secondary phase that does not contain any alcohol molecules, namely ice I $\text{H}_2\text{O}/\text{NH}_4\text{F}$. That is, all cages in the clathrate hydrate itself might be occupied; the occupancy of cages is between 79 and 100%.

Apart from the usual decrease in lattice constant linked to $\text{H}_2\text{O}/\text{NH}_4\text{F}$ mixtures as solid solutions,^{24,79} the addition of NH_4F induces small but significant structural differences in CHs.²⁴ This is related to the shortened $\text{N}-\text{H} \cdots \text{F}$ hydrogen bond, which is shorter by 4% compared to $\text{O}-\text{H} \cdots \text{O}$.⁷⁹ The full width at half maximum (FWHM) of the most prominent Bragg peak at $\approx 28^\circ$ of the ethanol + methanol sI $\text{H}_2\text{O}/\text{NH}_4\text{F}$ CH is 0.2° (Cu $\text{K}\alpha_1$; $\lambda = 0.15418$ nm, 77 K). For comparison, we estimate the FWHM of the same Bragg peak for a crystalline methane hydrate (sI) from Lunev *et al.*⁸⁰ (Cu $\text{K}\alpha_1$; $\lambda = 0.15418$ nm, 173 K) to be 0.3° . Evidently, despite some perturbation from the NH_4F addition, the CH is without a doubt fully crystalline.

Comparing the ratio of Bragg peak intensities at $\approx 23.0^\circ$ and $\approx 24.5^\circ$ to the ratio presented by Malkin *et al.*⁸¹ shows that an ice I stacking disordered by-phase is present. The secondary phase likely derives from ethanol being partially immiscible in the liquid solution at room temperature and hindering the entire liquid sample from transforming into CH. Shin *et al.*,²⁵ who had first synthesized this specific CH, tried to overcome this issue by using a higher concentration of the guest species and by immersing the frozen, grinded $\text{H}_2\text{O}/\text{NH}_4\text{F}$ mixture in an excess methanol/ethanol solution. Their

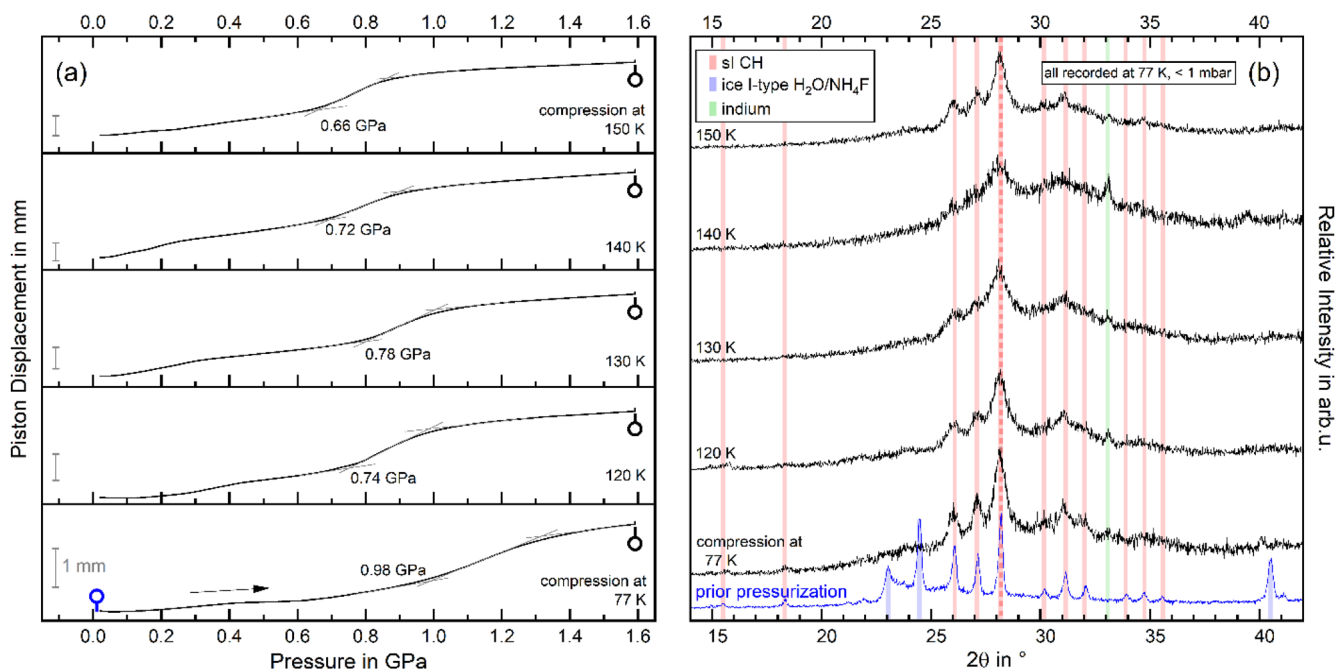


FIG. 1. (a) Dilatometric curves during isothermal compression from 0.02 to 1.6 GPa of crystalline ethanol + methanol sl CH at 77–150 K. Pressure-induced transformations are indicated by the change in slope, and the onset pressure is noted. Pin marks in black and blue refer to the positions at which x-ray diffractograms were taken, following recovery at 77 K in (b). (b) X-ray diffractograms of the crystalline ethanol + methanol sl CH at temperatures 77–150 K (from 0.02 to 1.6 GPa), following recovery at 77 K. Vertical colored lines mark typical reflex positions of sl CH (light red), ice I-type $\text{H}_2\text{O}/\text{NH}_4\text{F}$ (light blue), and indium remnants (light green). The dotted line (red/light red) shows the strongest, characteristic sl reflex, which is used for FWHM determination. All diffractograms were recorded at 77 K, <1 mbar.

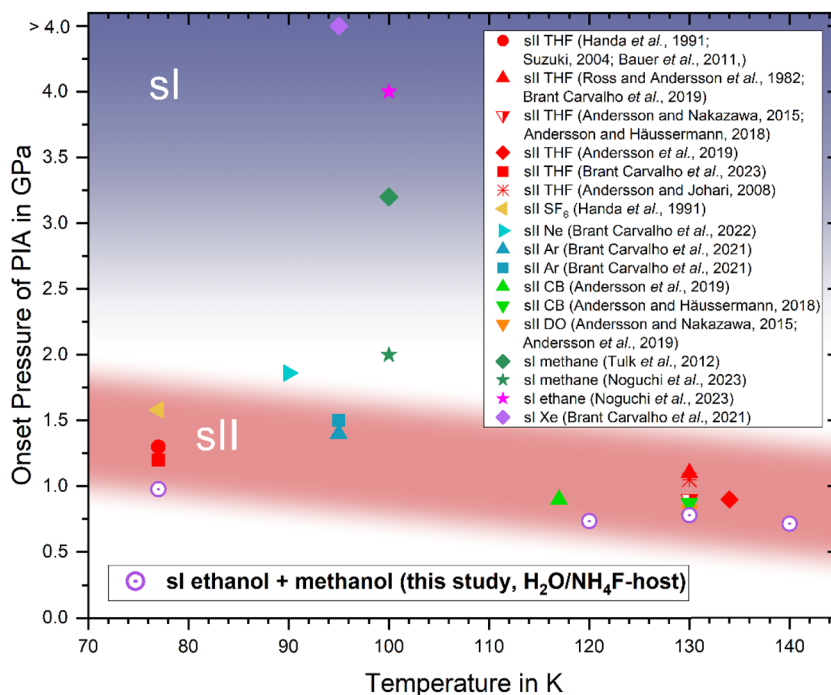


FIG. 2. Compilation of onset pressures of pressure-induced amorphization, both from past publications^{32,34–39,41–45,47,49,50} (pure- H_2O hosts only) and this study [$\text{H}_2\text{O}/73$ mol. %)- $\text{NH}_4\text{F}/27$ mol. %]. Red and blue areas show the trend of structure types sII and sl CHs, respectively.

diffractogram shows little to no difference in terms of by-phase formation compared to what our method yields. Yet, their by-phase is much less stacking-disordered than ours but mostly hexagonal. The pressure behavior of this phase mixture is studied at temperatures between 77 and 150 K up to 1.6 GPa. Changes in sample density indicating phase transitions are monitored *via in situ* dilatometry, and recovered samples are characterized *via ex situ* powder x-ray diffraction at 77 K at subambient pressure.

Piston-displacement curves starting from the crystalline CH at five different temperatures between 77 and 150 K of the sI CH are shown in Fig. 1(a). Piston-displacement curves can be converted to volume change by multiplication with the bore area (a circle of 8 mm inner diameter). By definition, the direction up corresponds to a densification in all figures in this work. Figure 1(a) indicates suddenly accelerated densification between 0.6 and 1.0 GPa, indicating a pressure-induced transformation. The transformation completes below 1.4 GPa. X-ray diffractograms of the high-pressure samples recovered after decompression at 77 K are shown in Fig. 1(b). They reveal a shift from narrow Bragg reflexes to broad peaks, confirming pressure-induced amorphization (PIA). In addition, the secondary phase, the ice-I-type $\text{H}_2\text{O}/\text{NH}_4\text{F}$ solid solution, amorphizes, with its amorphous halo hidden below the broad CH peaks. The amorphization of the secondary phase does not show up as a second densification event. It amorphizes simultaneously with the clathrate.

Unlike pure ice, the $\text{H}_2\text{O}/\text{NH}_4\text{F}$ solid solution does not undergo any crystalline-crystalline phase transition. Even small amounts of NH_4F as low as 2.5 mol. % suppress hydrogen-ordered phases^{82,83} such as ice II and expand the stability region of ice I-type phases.²⁷ A lack of sharp Bragg peaks associated with the secondary phase confirms the absence of crystalline-crystalline phase transitions in the $\text{H}_2\text{O}/\text{NH}_4\text{F}$ by-phase. The small densification in each compression curve between 0.2 and 0.4 GPa is attributed to a tiny amount of trapped air being squeezed out. No changes in the x-ray diffractogram are seen when recovering the sample at 0.4 GPa instead of 0.2 GPa.

The change in slope in the piston-displacement curve enables a determination of onset pressures for the pressure-induced transformation using the tangent intersection method [see tangents in Fig. 1(a)]. PIA sets in at 0.98 GPa at 77 K, then shifts to lower pressure at higher temperature. A comparison of the onset pressures of PIA in CHs is collected and summarized in Fig. 2. Compared to all other onset pressures for sI and sII clathrates in the literature, our specific CH begins to amorphize at a tremendously lower pressure (see Fig. 2). Other sI CHs undergo PIA at significantly higher pressure: sI methane hydrates amorphize at 3.2 GPa (100 K),^{39–41} while ethane hydrates undergo PIA at 4.0 GPa, and Xe hydrates at pressures above at least 4 GPa (95 K).³⁷ That is, the combination of NH_4F in the host and alcohol as a guest reduces the onset pressures by about 70%–75% to 25%–30% of previously reported pressures. Up until now, sII-THF CHs have been shown to exhibit the lowest onset pressure of all CHs, namely 1.2 GPa at 77 K.^{32,33,43,48} Here, the sI clathrate amorphizes at even lower pressure.

In terms of temperature, PIA is observed here on the sI CH up to at least 140 K, higher than reported before for all CHs with hydrophobic guests. The highest temperature at which the PIA of CH has been observed in past studies is 130–135 K. In this range,

THF,^{33,35,43,47,49,50} 1,3-dioxolane,^{33,34,42} and cyclobutanone^{33,42} CH undergo PIA at 0.9–1.1 GPa.

Figure 1(b) also shows that compression at different temperatures does not lead to an identical amorphous state. All pressurized samples show halo-like broadening near the typical sI reflex positions at 26.0°, 27.1°, 28.1°, 30.2°, 31.1°, and 32.0°. Yet, a variation in broadness linked to the degree of amorphicity, as given by the Debye–Scherrer relation,⁸⁴ is evident. Pressurization at temperatures of up to 140 K leads to an increase in peak broadness, which is related to an increase in amorphicity. At 150 K, these peaks become more narrow and more structured again. This hints at a mechanistic change in the pressure-induced transformation: While up to at least 140 K, PIA takes place at a higher and higher rate, at 150 K and above, amorphization slows down again, resulting in a less complete amorphization, i.e., lower amorphicity.

This development of peak broadness is quantified by the full width at half maximum (FWHM) of the strongest peak at 28.1°, as visualized in Fig. 3. Most remarkably, the amorphized sI CH is recoverable upon decompression at 77 K if previously compressed at 77–140 K. This renders it the only CH that can be recovered in its amorphous state without the requirement of the additional high-pressure annealing procedure presented by Suzuki⁴⁴ and Bauer *et al.*⁴⁵ To the best of our knowledge, it has even been impossible previously to recover amorphized sI clathrates.

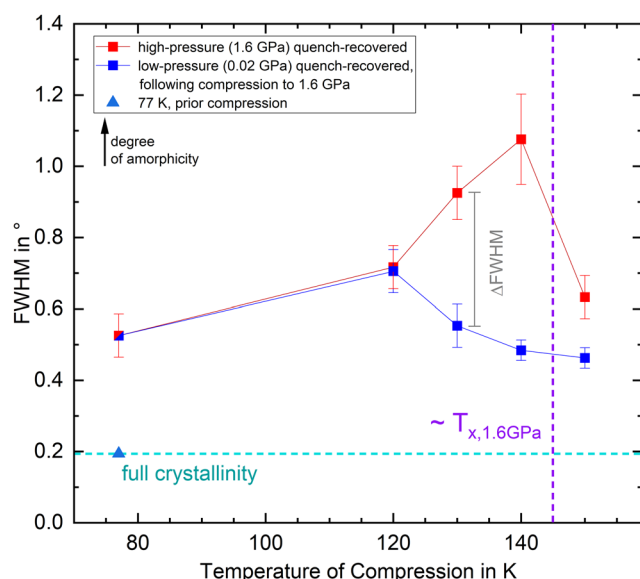


FIG. 3. Full Width at Half Maximum (FWHM) of the sI (halo) peak at 28.1° in the x-ray diffractograms of pressure-transformed ethanol + methanol CH as a function of the temperature of compression. High-pressure (1.6 GPa) quench-recovered CH, which has been decompressed at 77 K, is in red. The crossing of a crystallization temperature at 1.6 GPa $T_{x,1.6\text{GPa}}$ is sketched in a purple dashed line. Low-pressure (0.02 GPa) quench-recovered CH, which has been decompressed at the temperature of compression and then quenched to 77 K, is in blue. Only the data point in teal is prior to any compression and marks the minimal FWHM at full crystallinity in a turquoise dashed line. The difference in the full width at half maximum between the high- and low-pressure quench recovered pressure-transformed CHs, ΔFWHM , is markedly exemplary.

B. Recoverability: The downstroke transition

The amorphized CH even resists crystallization when decompressed at higher temperatures, up to at least 120 K. To demonstrate this, we have carried out decompression at 120, 130, 140, and 150 K with quenching to 77 K at 0.02 GPa. Figure 4(a) compares the volumetric curves for decompression at 77 K and at a higher temperature. The volume follows the same curve, no matter whether decompression is performed at 77 or 120 K. That is, the pressure-amorphized clathrate can be recovered both at 77 and 120 K at ambient pressure without crystallization. Starting at 130 K, decompression clearly leads to a state of lower density compared to decompression at 77 K. Evidently, partial crystallization is induced by a decrease in density when decompressing at 130 K. The difference in piston-displacement at 0.02 GPa [$d_{\text{expansion,decompression}}$, orange in Fig. 4(a)] reflects the volume change induced by the partial amorphous to crystalline transition upon decompression. The height of the step upon compression [$d_{\text{step,compression}}$, purple in Fig. 4(a)], on the other hand, indicates the volume change associated with the transition from fully crystalline to amorphous. The ratio of the two volumetric changes allows for defining and quantifying the reversibility of the amorphization upon decompression.

For amorphization at 140 K, the largest fraction crystallizes on the downstroke at 140 K. For 150 K, the volume difference at 0.02 GPa vanishes, which implies that already on the upstroke transition, distorted crystals are produced rather than amorphized

CH. Both for decompression at 77 and 150 K, the downstroke features a curved nature, especially below 0.2 GPa. We surmise that in this range, the densified, deformed crystals slowly start to progress back toward undeformed sl CH crystals. Yet, some degree of distortion is still retained down to ambient pressure, which is at the origin of the volume difference between the upstroke and downstroke transitions. This proves a mechanistic difference in the pressure-induced transformation at 150 K compared to 140 K and below. As PIA is no longer taking place during compression, no crystallization of an amorphized CH can occur. The finding of $d_{\text{expansion,decompression}} \approx 0$ should, in this case, not be confused with the recoverability of the amorphized CH; the amorphized clathrate just does not form in the upstroke.

The x-ray diffractograms of the samples decompressed at high-temperatures are shown in Fig. 4(b). They display varying degrees of amorphicity. The amorphicity, as gauged by the width of the peak at 28.1° , is graphed in Fig. 3. Up to 120 K, the degree of amorphicity is the same for low- and high-temperature decompression. For decompression temperatures of 130–150 K, the degree of amorphicity goes down, *i.e.*, back-transformation to sl CH crystals sets in upon decompression. The highest degree of amorphicity is reached when compressing at 140 K and decompressing at 77 K. Evidently, temperature increases aid PIA but also promote reversion to crystalline CH. Meanwhile, the absence of sharp Bragg peaks associated with the $\text{H}_2\text{O}/\text{NH}_4\text{F}$ by-phase shows that decompression

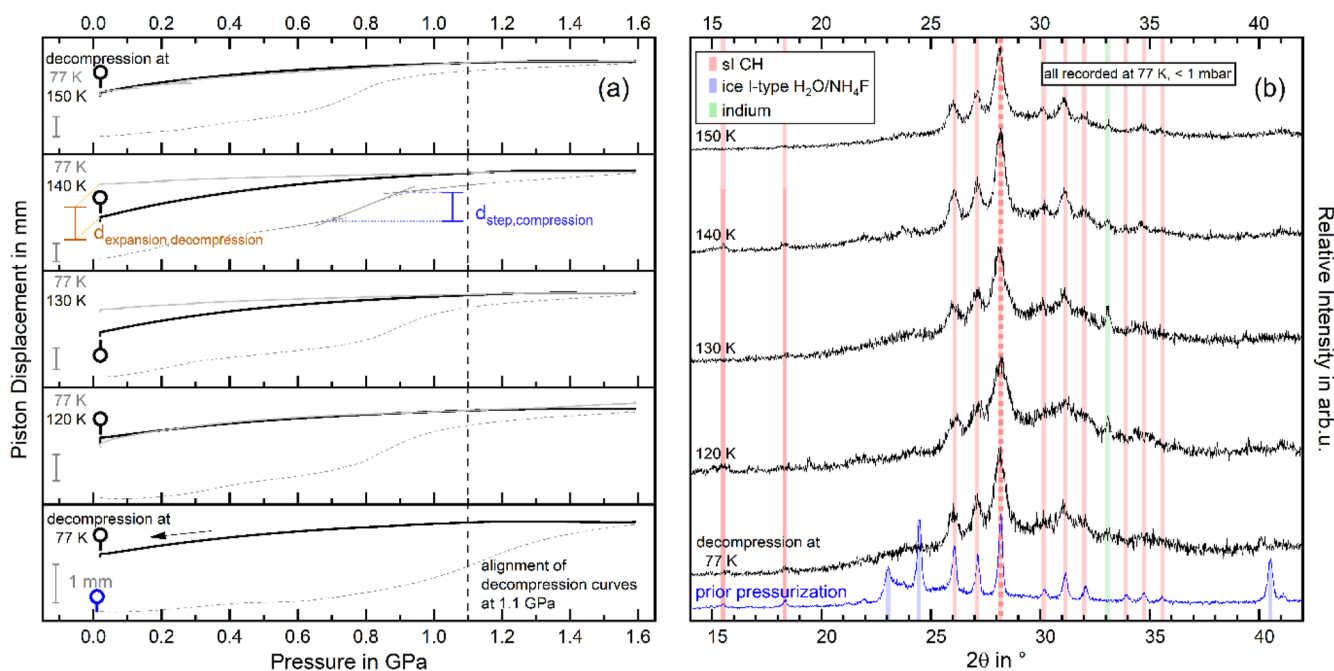


FIG. 4. (a) Dilatometric curves during isothermal decompression from 1.6 to 0.02 GPa of pressure-transformed ethanol + methanol sl CH at 77–150 K. Marks in black and blue refer to the recorded x-ray diffractogram, following recovery at 77 K, in (b). Dilatometric curves during compression from Fig. 1(a) are hinted weakly in black dotted lines. $d_{\text{step,compression}}$ and $d_{\text{expansion,decompression}}$ used for the determination of the reversibility quotient, Q_R , are sketched as exemplary. (b) X-ray diffractograms of the crystalline ethanol + methanol sl CH at 77 K, prior to any pressurization (blue), and decompressed pressure-transformed ethanol + methanol sl CH at temperatures 77–150 K (from 1.6 to 0.02 GPa), following recovery at 77 K. Vertical colored lines mark typical reflex positions of sl CH (light red), ice I-type $\text{H}_2\text{O}/\text{NH}_4\text{F}$ (light blue), and indium remnants (light green). The dotted line (red/light red) shows the strongest, characteristic sl reflex, which is used for FWHM determination. All diffractograms were recorded at 77 K, <1 mbar.

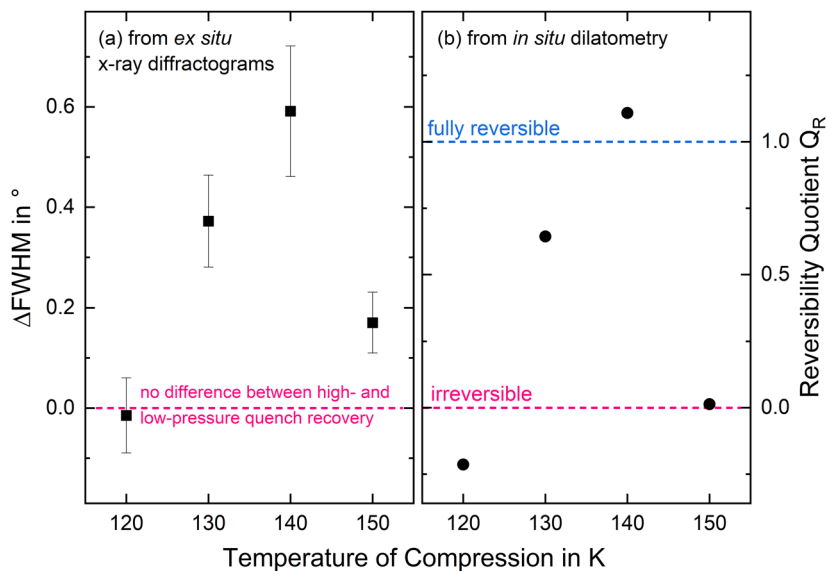


FIG. 5. (a) Difference in the full width at half maximum after high- and low-pressure quench recovery, ΔFWHM , determined from *ex situ* x-ray diffractograms. The value of 0 is marked by the pink dashed line. (b) Reversibility quotient, Q_R , as defined from volumetric data [see Fig. 4(a) and Eq. (1)]. Full reversibility and absolute irreversibility are marked as blue and pink dashed lines, respectively.

at either temperature between 77 and at least 150 K does not induce the crystallization of the by-phase.

The reversibility of the amorphization, *i.e.*, lack of crystallinity, is once again analyzed based on x-ray diffraction data in Fig. 5. While in Fig. 3, the absolute FWHM is plotted both for the downstroke transition at 77 K (high-pressure quench recovery) and the downstroke transition at a higher temperature (low-pressure quench recovery at 0.02 GPa), Fig. 5(a) focuses on the difference between the two, ΔFWHM . This difference in amorphicity is zero up to 120 K, proving full recoverability up to this temperature. Up to 140 K, ΔFWHM then increases, which is a result of higher amorphicity after the upstroke at 140 K but back-crystallization in the downstroke at 140 K. Reversibility is clearly lost at 140 K. From 140 to 150 K, ΔFWHM drops significantly, which is linked to the lower degree of amorphization after the upstroke at 150 K/1.6 GPa. Instead of PIA, pressure-induced crystal deformation and densification occur at 150 K. All in all, x-ray diffractograms prove the loss in crystallinity for the upstroke up to 140 K and the recoverability of the amorphous CH up to 120 K.

The crystallization of amorphized CHs upon decompression is not only reflected in the *ex situ* x-ray diffractograms but also in the *in situ* dilatometric curves in Fig. 4(a). As indicated earlier, the step height for the upstroke transition and the piston-displacement difference between two downstroke curves can be employed to quantify reversibility [both are exemplarily marked in Fig. 4(a)]. We define the reversibility quotient, Q_R , on the basis of expansion upon decompression and the compaction step upon compression as

$$Q_R = \frac{d_{\text{expansion, decompression}}}{d_{\text{step, compression}}} \quad (1)$$

Q_R in Fig. 5(b), defined from dilatometry data, shows a remarkable resemblance to ΔFWHM in Fig. 5(a), defined from x-ray

diffractograms. This agreement between the *ex situ* x-ray diffraction and *in situ* dilatometric methods demonstrates that amorphization/crystallization can be identified equally from volumetric and crystallographic data. Both methods indicate the remarkable stability of the amorphous $\text{H}_2\text{O}/\text{NH}_4\text{F}$ -alcohol CHs at 77 K. In other words, the combination of the use of NH_4F in the host lattice and the use of hydrophilic alcoholic guests allows for unprecedented destabilization of the crystalline host network, so that PIA takes place at surprisingly low pressures. Furthermore, amorphized clathrates of this composition are highly resistant against crystallization—much more resistant than other amorphized clathrates studied in the past. The densifying transformation is already fully reversible upon decompression at 140 K in terms of dilatometric curves, and no new crystalline Bragg peaks linked to the secondary phase appear. This demonstrates that the PIA of the ice I-like secondary phase is negligible compared to the PIA of the CH.

C. Molecular dynamics simulations

In order to rationalize such findings, we have also carried out MD simulations with and without NH_4F and with polar alcohol guests or non-polar hydrocarbon guests of similar size. These four systems were simulated at 77 K under increasing pressure. Switching between alcohol and hydrocarbon guests of comparable size provides insight into the effect of the polar vs non-polar character of the guest. More specifically, we employed one ethanol molecule in each large cage (T) and one molecule of methanol in each small cage (D) for the polar guests and propane and ethane in T and D, respectively, for non-polar guests. Using H_2O -only and partial NH_4F -substitution in the host structure offers an evaluation of the effect of NH_4F . The mixing ratio of NH_4F closely resembles the experimental one. By combining these variations, an

interplay between NH_4F -substitution and alcoholic guests is singled out. Monitoring the cell constant under increasing pressure in the unit cell shows the effect the different components have on the collapse of the crystalline clathrate in Fig. 6(a). This analysis closely resembles experimental dilatometry. In the simulations, pressure is increased step-by-step, whereas in experiments, we continuously increase pressure. All curves first show an equilibration of the cell

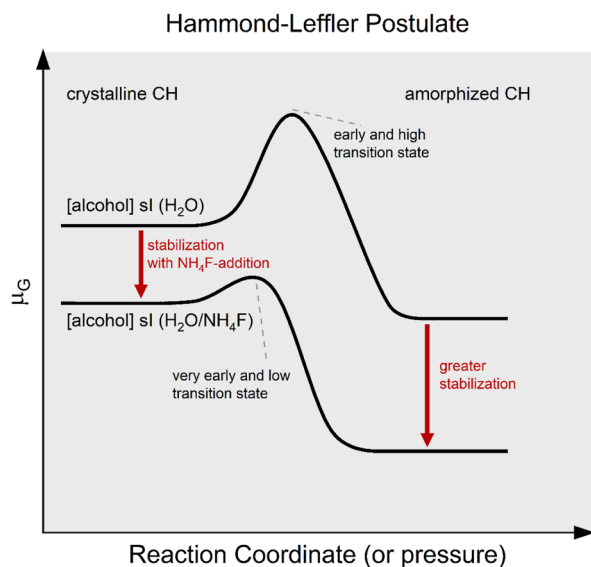
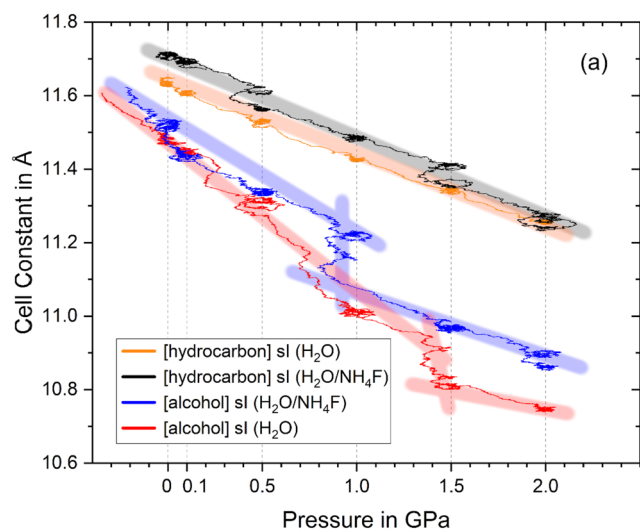


FIG. 6. (a) Simulated cell constant of sl unit cells of four different combinations, differing in guest molecule (in square brackets) and/or host composition upon pressure increase at 77 K. Each data point is symmetrically averaged over 1001 neighboring data points. Pressure is applied stepwise (1 atm, 0.1, 0.5, 1.0, 1.5, and 2.0 GPa) and marked by gray dashed lines. Estimated trend lines act as a guide to the eye and highlight significant changes in slope. (b) Schematic representation of the chemical potential μ_G based on the Hammond postulate applied to the pressure-induced mechanical collapse (comparable to PIA) of pure- H_2O and NH_4F -containing CHs with alcoholic guests.

constant to the new pressure conditions, after which the pressure oscillates about the target value. The associated time evolution of the applied pressure as a function of simulation time is provided in Fig. SM1 of the supplementary material.

Even though neither amorphization nor an amorphous structure alone can be properly described in such a small system, the collapse of the crystalline structure in this unit cell is comparable to an amorphization. The pressure it takes to cause a collapse of the crystalline cages, therefore, mirrors the onset pressures of the PIA of different CHs. Just like in the experiment, CHs with alcoholic guests collapse at significantly lower pressures compared to the same systems with hydrocarbon guests. In fact, regardless of host composition, alkane-filled CHs show a near-linear decrease in cell constant [cf. Fig. 6(a), black and orange line], without any change in slope to indicate a sudden collapse. Evidently, the repulsive force between guest and host stabilizes the cages from within. By contrast, alcohol-filled CHs not only show a stronger decrease in size but also exhibit a change in slope and an abrupt decrease in the cell constant as the crystalline cages collapse [cf. Fig. 6(a), blue and red lines]. Most importantly, these findings reflect what the experimental data have shown in this study. An alcohol-filled NH_4F -substituted CH loses its crystalline structure at significantly lower pressures than CH with a H_2O -only host structure and non-polar guests. Furthermore, even before collapse is reached, alcohol-filled CHs show a lower cell constant than alkane-filled CHs. This is likely linked to alcohol's ability to form hydrogen bonds with the host structure, NH_4F -containing^{24,25,85} or not.^{16,86–88} Shin *et al.*²⁵ have suggested that these (transient) hydrogen bonds between alcoholic guests and the host structure could reduce the cage size in NH_4F -containing CHs, methanol most of all.

While non-polar hydrocarbon guests repulse the cage from within, polar alcoholic guests pull in the host structure. In fact, this ability to form hydrogen bonds with the host structure is the reason for the instability of pure- H_2O CHs with alcoholic guests.^{86–88} As guest–host bonds are formed, the host's hydrogen-bond network is destabilized and partially breaks. By contrast, NH_4F -containing CHs withstand the destabilization of the host-network despite strong interactions with the alcoholic guest.^{24,25}

The effect of NH_4F on the collapse of alcohol containing CHs is evident in Fig. 6(a). The pure- H_2O CH with alcoholic guests experiences sudden densification as 1.5 GPa is reached. The addition of NH_4F to the systems induces a collapse at 0.9 GPa. Apart from affecting the pressure of collapse, NH_4F does not significantly influence the lattice parameters.⁸⁹ That is, NH_4F in the host lowers the pressure of collapse. In experiments, crystalline alcohol CHs are very hard to make and have remained elusive for a very long time. This is because polar guests make the crystalline CH highly unstable, to the point of thermodynamic impossibility.^{86–88} Clearly, the addition of NH_4F to the alcohol-containing CH has proven to enhance thermodynamic stability.^{24,25} This stabilization in terms of the chemical potential μ_G is indicated by the red arrow at the left in Fig. 6(b), which sketches the reaction coordinate for PIA of alcohol CH both with and without NH_4F . In spite of this higher thermodynamic stability, our simulations show an earlier pressure-induced collapse for the NH_4F -containing CH with alcoholic guests, feigning lower stability. This lower stability against pressure increases is kinetic in origin and can be reconciled based on the Hammond–Leffler

postulate.⁹⁰ In Fig. 6(b), the barrier against amorphization is much lower for the CH containing NH_4F , reflecting the lower pressure of collapse in Fig. 6(a). A lower and earlier barrier necessitates a more exergonic transition, according to the Hammond–Leffler principle. That is, in the presence of NH_4F , the amorphized clathrate is more strongly stabilized than in its absence. This is indicated by the longer red arrow for the amorphized CH in Fig. 6(b). The pure- H_2O alcohol containing CH experiences a less early transition state because of its less exergonic nature. That is, there is an anti-correlation between exergonicity and barrier height, and hence also kinetics. The larger stabilization of the amorphous clathrate containing NH_4F is plausible considering that there is an additional contribution to the exergonic transition that originates from the mixing entropy in the presence of NH_4F . This mixing entropy is absent for the alcohol clathrates without NH_4F . According to Hammond’s postulate, a steeper fall in μ_G is linked to a lower barrier and a higher transformation rate. This causes the transition to shift to lower pressures in the presence of NH_4F , in spite of the increased stability of crystalline CHs.

IV. CONCLUSIONS

We have investigated ethanol + methanol clathrate hydrates of cubic structure I, which contain NH_4F in the host lattice. Our main focus is on their stability against pressure-transformations in cryo-conditions. We reveal that the CH undergoes pressure-induced amorphization (PIA) like many other CHs, but it does so at incredibly low pressure: at 77 K, PIA sets in at 0.98 GPa. Other sI clathrates, e.g., methane hydrates, experience this transition typically between 2 and 4 GPa. Even sII CHs, which amorphize at significantly lower pressures, such as sII THF CHs, need at least 1.2 GPa.⁴⁸ These low PIA onset pressures persist at 130 K, where PIA sets in at 0.78 GPa, as opposed to 0.9 GPa for sII THF CHs.^{34,35} However, even beyond, while PIA has never been reported for any CHs above 135 K,³³ this ethanol + methanol CH amorphizes at 0.72 GPa at 140 K.

All samples amorphized at different temperatures are recoverable at 77 K, in contrast to many other amorphized CHs. This is a unique feature of the alcohol-ammonium fluoride CH studied here. No other amorphized sI CH could be recovered to ambient pressure so far, to the best of our knowledge. While many pressure-amorphized CHs cannot be recovered to ambient pressure at all, some amorphized sII CHs require an elaborate high-pressure annealing procedure.^{44,45} The clathrate investigated here is unique since it can be recovered without any elaborate procedures but by simple decompression. X-ray diffraction of the recovered amorphous CH reveals a variation in the degree of amorphization. With increasing temperature, a higher degree of amorphization is reached. Likely, the lack of kinetic energy at low temperatures hinders a transformation to a state of higher amorphization. A comparison to pure H_2O can be drawn, which, after low temperature compression, still holds crystalline remnants after PIA.^{53–55} Only annealing to elevated temperatures allows a transformation to its fully amorphous form.^{57,91} Similarly, for the CHs of this study, similar states might be reached upon compression at elevated temperature, with a comparable effect to temperature-annealing at higher pressure. Remarkably, PIA is fully irreversible up to temperatures of at least 120 K for the alcohol- NH_4F CH. As for reversibility, recovery at 77 K has proven to show no changes in the sample, which is confirmed both from

in situ dilatometry and *ex situ* x-ray diffraction. At 150 K, a mechanistic change is observed. While there is still a step-like densification of the sI CH, the x-ray diffractograms indicate broader peaks and a lower degree of amorphicity than at 140 K. Both decompressions at 77 and 150 K yield the same x-ray pattern featuring broadened Bragg peaks. That is, densified and deformed crystals are obtained rather than amorphized CH. By contrast, the CH after amorphization at 140 K reverts back to the crystalline CH when decompressed at 140 K but remains amorphized when decompressed at 77 K. The highest degree of amorphicity is reached when compressing at 140 K and decompressing at 77 K. True PIA is evident from the dilatometric experiments both for the CHs studied here and “simple” tetrahydrofuran (THF) CHs. In terms of x-ray diffractograms, amorphized THF CHs feature broader halos^{44,45} compared to the ones here. The smaller FWHM in the amorphized $\text{H}_2\text{O}/\text{NH}_4\text{F}$ -alcohol CH’s diffractogram indicates some remnants of order. This likely derives from the alcohol’s polarity and capability to form hydrogen bonds with the host structure.^{16,86–88} Alcohol has been shown to hydrogen bond especially strongly with F^- and NH_4^+ in the host structure of modified CHs.^{24,25,85} These strong hydrogen bonds likely persist even through PIA and maintain some long range order within the amorphous matrix.

MD simulations of sI CHs differing in terms of guest and host composition help uncover the effect either factor has on the system’s stability. Unsurprisingly, alcoholic guests, with their polar character, promote the pressure-induced collapse, while non-polar hydrocarbon guests stabilize the cages from within to withstand collapse over a wider pressure range. The Hammond–Leffler postulate is utilized to help describe the effect of NH_4F on alcohol-filled CHs: The addition induces stabilization both in the crystalline and collapsed states, in comparison to a pure- H_2O CH. This stabilization is higher in the case of the amorphized CH (due to the additional contribution of mixing entropy), which causes an earlier and lower transition state and a steeper drop in chemical potential during the pressure-induced collapse of NH_4F -containing CHs with alcoholic guests. This is reflected by the lower pressure needed for collapse in the simulation. This way, NH_4F aids pressure-induced amorphization, regardless of structure or the presence of a guest. Even for a guest-free $\text{H}_2\text{O}/\text{NH}_4\text{F}$ solid solution of ice-I-type structure, PIA sets in earlier at 0.98 GPa,²⁷ as opposed to 1.2 GPa for pure- H_2O ice I.²⁷

Either way, this ethanol + methanol sI $\text{H}_2\text{O}/\text{NH}_4\text{F}$ is the first from this family of unusual CHs to be studied under pressure. The results mentioned earlier are also quite unique when compared with other sI CHs. In future work, CHs with more traditional, non-polar guests, but an NH_4F -containing framework, should be focused on. A few candidates come to mind, such as a sII THF NH_4F -containing CH or a sI methane NH_4F -containing CH.³⁰ Following our findings here, their PIA would be expected to be at a slightly lower pressure than their NH_4F -free counterpart. In addition, experiments on alcohol CHs free of NH_4F would be desirable. Yet, methanol hydrates are considered unstable and, therefore, regarded by many as impossible to synthesize.^{86–88} A number of claims of successful methanol CH syntheses by vapor co-deposition^{92–94} have been reported. However, others point out the lack of evidence for crystallinity in these alleged methanol CHs.^{16,25} sI ethanol hydrates have been synthesized by vapor-deposition⁹⁵ but have not yet been pressurized. This pure- H_2O CH represents the missing link between

pure-H₂O CH with traditionally non-polar guests and the ethanol + methanol NH₄F-containing CH from this study.

SUPPLEMENTARY MATERIAL

The supplementary material includes a visualization of the time evolution of the applied pressure as a function of the simulation time of each simulated system in Fig. SM1.

ACKNOWLEDGMENTS

We gratefully acknowledge financial support from the Austrian Science Fund (FWF), Project No. P36634. We are indebted to Stefan Arzbacher for his discussion of the paper.

AUTHOR DECLARATIONS

Conflict of Interest

The authors have no conflicts to disclose.

Author Contributions

Lilli-Ruth Fidler: Conceptualization (supporting); Data curation (lead); Formal analysis (lead); Investigation (lead); Writing – original draft (lead); Writing – review & editing (equal). **Paul Posch:** Data curation (supporting); Investigation (supporting). **Johannes Klocker:** Data curation (supporting). **Thomas S. Hofer:** Conceptualization (supporting); Supervision (lead); Writing – review & editing (supporting). **Thomas Loerting:** Conceptualization (lead); Funding acquisition (lead); Methodology (lead); Supervision (lead); Writing – original draft (equal); Writing – review & editing (lead).

DATA AVAILABILITY

The data that support the findings of this study are available from the corresponding author upon reasonable request.

REFERENCES

- 1 E. D. Sloan, Jr., C. A. Koh, and C. A. Koh, *Clathrate Hydrates of Natural Gases* (CRC Press, 2007).
- 2 C. A. Koh, E. D. Sloan, A. K. Sum, and D. T. Wu, “Fundamentals and applications of gas hydrates,” *Annu. Rev. Chem. Biomol. Eng.* **2**, 237–257 (2011).
- 3 N. Dabrowski, C. Windmeier, and L. R. Oellrich, “Purification of natural gases with high CO₂ content using gas hydrates,” *Energy Fuels* **23**, 5603–5610 (2009).
- 4 A. Gupta *et al.*, “Hydrogen clathrates: Next generation hydrogen storage materials,” *Energy Storage Mater.* **41**, 69–107 (2021).
- 5 I. Dincer and C. Zamfirescu, “Fossil fuels and alternatives,” in *Advanced Power Generation Systems* (Elsevier Inc., 2014), pp. 95–141.
- 6 S. Y. Lee and G. D. Holder, “Methane hydrates potential as a future energy source,” *Fuel Process. Technol.* **71**, 181–186 (2001).
- 7 K. A. Kvenvolden, “Methane hydrate—A major reservoir of carbon in the shallow geosphere?,” *Chem. Geol.* **71**, 41–51 (1988).
- 8 E. D. Sloan, Jr., C. A. Koh, and C. A. Koh, *Clathrate Hydrates of Natural Gases. Chemical Industries* (CRC Press, 2007).

- 9 Y. Lee, D. Seo, S. Lee, and Y. Park, “Advances in nanomaterials for sustainable gas separation and storage: Focus on clathrate hydrates,” *Acc. Chem. Res.* **56**, 3111–3120 (2023).
- 10 J. A. Ripmeester and S. Alavi, *Clathrate Hydrates—Molecular Science and Characterization: 2 Volumes* (Wiley-VCH Verlag, 2022).
- 11 K. Yasuda, S. Takeya, M. Sakashita, H. Yamawaki, and R. Ohmura, “Binary ethanol–methane clathrate hydrate formation in the system CH₄–C₂H₅OH–H₂O: Confirmation of structure II hydrate formation,” *J. Phys. Chem. C* **113**, 12598–12601 (2009).
- 12 K. Yasuda, S. Takeya, M. Sakashita, H. Yamawaki, and R. Ohmura, “Characterization of the clathrate hydrate formed with methane and propan-1-ol,” *Ind. Eng. Chem. Res.* **48**, 9335–9337 (2009).
- 13 K. Udachin, S. Alavi, and J. A. Ripmeester, “Communication: Single crystal x-ray diffraction observation of hydrogen bonding between 1-propanol and water in a structure II clathrate hydrate,” *J. Chem. Phys.* **134**, 121104 (2011).
- 14 R. Ohmura, S. Takeya, T. Uchida, and T. Ebinuma, “Clathrate hydrate formed with methane and 2-propanol: Confirmation of structure II hydrate formation,” *Ind. Eng. Chem. Res.* **43**, 4964–4966 (2004).
- 15 Y. Park, M. Cha, W. Shin, H. Lee, and J. A. Ripmeester, “Spectroscopic observation of critical guest concentration appearing in tert-butyl alcohol clathrate hydrate,” *J. Phys. Chem. B* **112**, 8443–8446 (2008).
- 16 K. Shin *et al.*, “Methanol incorporation in clathrate hydrates and the implications for oil and gas pipeline flow assurance and icy planetary bodies,” *Proc. Natl. Acad. Sci. U. S. A.* **110**, 8437–8442 (2013).
- 17 D. W. Davidson, S. R. Gough, J. A. Ripmeester, and H. Nakayama, “The effect of methanol on the stability of clathrate hydrates,” *Can. J. Chem.* **59**, 2587–2590 (1981).
- 18 J. P. Devlin, “Catalytic activity of methanol in all-vapor subsecond clathrate-hydrate formation,” *J. Chem. Phys.* **140**, 164505 (2014).
- 19 G. McLaurin, K. Shin, S. Alavi, and J. A. Ripmeester, “Antifreezes act as catalysts for methane hydrate formation from ice,” *Angew. Chem.* **126**, 10597–10601 (2014).
- 20 S. Bobev and K. T. Tait, “Methanol-inhibitor or promoter of the formation of gas hydrates from deuterated ice?,” *Am. Mineral.* **89**, 1208–1214 (2004).
- 21 J. Amtawong *et al.*, “Propane clathrate hydrate formation accelerated by methanol,” *J. Phys. Chem. Lett.* **7**, 2346–2349 (2016).
- 22 N. Bjerrum, “Structure and properties of ice,” *Science* **115**, 385–390 (1952).
- 23 V. Buch *et al.*, “Clathrate hydrates with hydrogen-bonding guests,” *Phys. Chem. Chem. Phys.* **11**, 10245–10265 (2009).
- 24 K. Shin *et al.*, “Crystal engineering the clathrate hydrate lattice with NH₄F,” *CrystEngComm* **16**, 7209–7217 (2014).
- 25 K. Shin, I. L. Moudrakovski, C. I. Ratcliffe, and J. A. Ripmeester, “Managing hydrogen bonding in clathrate hydrates by crystal engineering,” *Angew. Chem.* **129**, 6267–6271 (2017).
- 26 L. C. Labowitz and E. F. Westrum, “A thermodynamic study of the system ammonium fluoride–water. II. The solid solution of ammonium fluoride in ice,” *J. Phys. Chem.* **65**, 408–414 (1961).
- 27 Z. Sharif, “New insights into water’s phase diagram using ammonium fluoride,” Ph.D. thesis, University College London, 2020.
- 28 J. Kim, K. Shin, S. Alavi, and J. A. Ripmeester, “Effect of methanol guests on thermal properties of NH₄F-doped THF clathrate hydrate,” *Energy Fuels* **36**, 10504–10511 (2022).
- 29 S. Park, D. Lim, Y. Seo, and H. Lee, “Incorporation of ammonium fluoride into clathrate hydrate lattices and its significance in inhibiting hydrate formation,” *Chem. Commun.* **51**, 8761 (2015).
- 30 B. Lee, K. Shin, S. Alavi, and J. A. Ripmeester, “Effect of ammonium fluoride doping on nitrogen, oxygen, and methane clathrate hydrates,” *Energy Fuels* **36**, 11123–11131 (2022).
- 31 D. H. Kim, K. H. Park, M. Cha, and J. H. Yoon, “Structure determination of clathrate hydrates formed from alcoholic guests with NH₄F and H₂O,” *Korean J. Chem. Eng.* **39**, 2211–2216 (2022).
- 32 Y. P. Handa, J. S. Tse, D. D. Klug, and E. Whalley, “Pressure-induced phase transitions in clathrate hydrates,” *J. Chem. Phys.* **94**, 623–627 (1991).

- ³³P. Andersson and R. G. Ross, "Effect of guest molecule size on the thermal conductivity and heat capacity of clathrate hydrates," *J. Phys. C: Solid State Phys.* **16**, 1423–1432 (1983).
- ³⁴O. Andersson and Y. Nakazawa, "Transitions in pressure collapsed clathrate hydrates," *J. Phys. Chem. B* **119**, 3846–3853 (2015).
- ³⁵O. Andersson and U. A. Häussermann, "A second glass transition in pressure collapsed type II clathrate hydrates," *J. Phys. Chem. B* **122**, 4376–4384 (2018).
- ³⁶P. H. B. Brant Carvalho *et al.*, "Exploring high-pressure transformations in low-Z (H₂, Ne) hydrates at low temperatures," *Crystals* **12**, 9 (2021).
- ³⁷P. H. B. Brant Carvalho *et al.*, "Pressure-induced amorphization of noble gas clathrate hydrates," *Phys. Rev. B* **103**, 064205 (2021).
- ³⁸P. H. B. Brant Carvalho *et al.*, "Structural investigation of three distinct amorphous forms of Ar hydrate," *RSC Adv.* **11**, 30744–30754 (2021).
- ³⁹C. A. Tulk, D. D. Klug, J. J. Molaison, A. M. Dos Santos, and N. Pradhan, "Structure and stability of an amorphous water-methane mixture produced by cold compression of methane hydrate," *Phys. Rev. B* **86**, 054110 (2012).
- ⁴⁰N. J. English and J. S. Tse, "Pressure-induced amorphization of methane hydrate," *Phys. Rev. B* **86**, 104109 (2012).
- ⁴¹Note that Noguchi *et al.* have observed PIA of methane hydrates between 2 and 3.2 GPa, 100 K. N. Noguchi *et al.*, "Direct observation of pressure-induced amorphization of methane/ethane hydrates using Raman and infrared spectroscopy," *Phys. Chem. Chem. Phys.* **25**, 22161–22170 (2023).
- ⁴²O. Andersson *et al.*, "Transitions in pressure-amorphized clathrate hydrates akin to those of amorphous ices," *J. Chem. Phys.* **151**, 014502 (2019).
- ⁴³R. G. Ross and P. Andersson, "Clathrate and other solid phases in the tetrahydrofuran–water system: Thermal conductivity and heat capacity under pressure," *Can. J. Chem.* **60**, 881–892 (1982).
- ⁴⁴Y. Suzuki, "Evidence of pressure-induced amorphization of tetrahydrofuran clathrate hydrate," *Phys. Rev. B* **70**, 172108 (2004).
- ⁴⁵M. Bauer, D. M. Töbrens, E. Mayer, and T. Loerting, "Pressure-amorphized cubic structure II clathrate hydrate: Crystallization in slow motion," *Phys. Chem. Chem. Phys.* **13**, 2167–2171 (2011).
- ⁴⁶G. P. Johari and S. J. Jones, "Transformation of an ice clathrate and hexagonal ice on compression at 77 K," *Philos. Mag. B* **54**, 311–315 (1986).
- ⁴⁷P. H. B. Brant Carvalho *et al.*, "Elucidation of the pressure induced amorphization of tetrahydrofuran clathrate hydrate," *J. Chem. Phys.* **150**, 204506 (2019).
- ⁴⁸P. H. B. Brant Carvalho *et al.*, "Neutron scattering study of polyamorphic THF-17(H₂O)-toward a generalized picture of amorphous states and structures derived from clathrate hydrates," *Phys. Chem. Chem. Phys.* **25**, 14981–14991 (2023).
- ⁴⁹O. Andersson and G. P. Johari, "Nature of the pressure-induced collapse of an ice clathrate by dielectric spectroscopy," *J. Chem. Phys.* **129**, 234505 (2008).
- ⁵⁰O. Andersson and G. P. Johari, "Collapse of an ice clathrate under pressure observed via thermal conductivity measurements," *Phys. Rev. B* **78**, 174201 (2008).
- ⁵¹O. Mishima, L. D. Calvert, and E. Whalley, "'Melting ice' I at 77 K and 10 kbar: A new method of making amorphous solids," *Nature* **310**, 393–395 (1984).
- ⁵²T. Loerting *et al.*, "Amorphous ice: Stepwise formation of very-high-density amorphous ice from low-density amorphous ice at 125 K," *Phys. Rev. Lett.* **96**, 025702 (2006).
- ⁵³M. Seidl, K. Amann-Winkel, P. H. Handle, G. Zifferer, and T. Loerting, "From parallel to single crystallization kinetics in high-density amorphous ice," *Phys. Rev. B* **88**, 174105 (2013).
- ⁵⁴M. Seidl, A. Fayer, J. N. Stern, G. Zifferer, and T. Loerting, "Shrinking water's no man's land by lifting its low-temperature boundary," *Phys. Rev. B* **91**, 144201 (2015).
- ⁵⁵C. M. Tonauser, M. Seidl-Nigsch, and T. Loerting, "High-density amorphous ice: Nucleation of nanosized low-density amorphous ice," *J. Phys.: Condens. Matter* **30**, 034002 (2018).
- ⁵⁶O. Mishima, L. D. Calvert, and E. Whalley, "An apparently first-order transition between two amorphous phases of ice induced by pressure," *Nature* **314**, 76–78 (1985).
- ⁵⁷R. J. Nelmes *et al.*, "Annealed high-density amorphous ice under pressure," *Nat. Phys.* **2**, 414–418 (2006).
- ⁵⁸T. Loerting, C. Salzmann, I. Kohl, E. Mayer, and A. Hallbrucker, "A second distinct structural 'state' of high-density amorphous ice at 77 K and 1 bar," *Phys. Chem. Chem. Phys.* **3**, 5355–5357 (2001).
- ⁵⁹O. Mishima, "Relationship between melting and amorphization of ice," *Nature* **384**, 546–549 (1996).
- ⁶⁰J. S. Loveday and R. J. Nelmes, "High-pressure gas hydrates," *Phys. Chem. Chem. Phys.* **10**, 937–950 (2008).
- ⁶¹J. S. Tse, D. D. Klug, J. A. Ripmeester, S. Desgreniers, and K. Lagarec, "The role of non-deformable units in pressure-induced reversible amorphization of clathrasils," *Nature* **369**, 724–727 (1994).
- ⁶²C. M. Tonauser, L.-R. Fidler, J. Giebelmann, K. Yamashita, and T. Loerting, "Nucleation and growth of crystalline ices from amorphous ices," *J. Chem. Phys.* **158**, 141001 (2023).
- ⁶³H. Tanaka and Y. Amano, "Pressure-induced amorphization of clathrate hydrates," *Mol. Phys.* **100**, 2183–2188 (2002).
- ⁶⁴J. S. Loveday *et al.*, "Stable methane hydrate above 2 GPa and the source of Titan's atmospheric methane," *Nature* **410**, 661–663 (2001).
- ⁶⁵J. Bachler, I. Daidone, L. Zanetti-Polzi, and T. Loerting, "Tuning the low-temperature phase behavior of aqueous ionic liquids," *Phys. Chem. Chem. Phys.* **26**, 9741–9753 (2024).
- ⁶⁶C. M. Tonauser *et al.*, "Strategies to obtain highly ordered deuterated ices presented on the example of ice XIV," *PNAS Nexus* **2**, pgad418 (2023).
- ⁶⁷C. M. Tonauser, K. Yamashita, L. del Rosso, M. Celli, and T. Loerting, "Enthalpy change from pure cubic ice I_c to hexagonal ice I_h," *J. Phys. Chem. Lett.* **14**, 5055–5060 (2023).
- ⁶⁸J. Giebelmann, J. Bachler, and T. Loerting, "Glass polymorphism in hyperquenched aqueous LiCl solutions," *J. Phys. Chem. B* **127**, 3463–3477 (2023).
- ⁶⁹F. Izquierdo-Ruiz, A. Otero-de-la-Roza, J. Contreras-García, O. Prieto-Ballesteros, and J. M. Recio, "Effects of the CO₂ guest molecule on the sI clathrate hydrate structure," *Materials* **9**, 777 (2016).
- ⁷⁰J. D. Bernal and R. H. Fowler, "A theory of water and ionic solution, with particular reference to hydrogen and hydroxyl ions," *J. Chem. Phys.* **1**, 515–548 (1933).
- ⁷¹F. Spiegelman *et al.*, "Density-functional tight-binding: Basic concepts and applications to molecules and clusters," *Adv. Phys.: X* **5**, 1710252 (2020).
- ⁷²M. Elstner *et al.*, "Self-consistent-charge density-functional tight-binding method for simulations of complex materials properties," *Phys. Rev. B* **58**, 7260 (1998).
- ⁷³B. Hourahine *et al.*, "DFTB+, a software package for efficient approximate density functional theory based atomistic simulations," *J. Chem. Phys.* **152**, 124101 (2020).
- ⁷⁴M. Gaus, A. Goez, and M. Elstner, "Parametrization and benchmark of DFTB3 for organic molecules," *J. Chem. Theory Comput.* **9**, 338–354 (2013).
- ⁷⁵M. Kubillus, T. Kubař, M. Gaus, J. Řezáč, and M. Elstner, "Parameterization of the DFTB3 method for Br, Ca, Cl, F, I, K, and Na in organic and biological systems," *J. Chem. Theory Comput.* **11**, 332–342 (2015).
- ⁷⁶L. Verlet, "Computer 'experiments' on classical fluids. I. Thermodynamical properties of Lennard-Jones molecules," *Phys. Rev.* **159**, 98–103 (1967).
- ⁷⁷G. Bussi, D. Donadio, and M. Parrinello, "Canonical sampling through velocity rescaling," *J. Chem. Phys.* **126**, 014101 (2007).
- ⁷⁸H. J. C. Berendsen, J. P. M. Postma, W. F. Van Gunsteren, A. Dinola, and J. R. Haak, "Molecular dynamics with coupling to an external bath," *J. Chem. Phys.* **81**, 3684–3690 (1984).
- ⁷⁹A. K. Lyashchenko and G. G. Malenkov, "X-ray investigation of ammonium fluoride-ice systems," *J. Struct. Chem.* **10**, 616–617 (1970).
- ⁸⁰I. Lunev *et al.*, "Advances in the study of gas hydrates by dielectric spectroscopy," *Molecules* **26**, 4459 (2021).
- ⁸¹T. L. Malkin *et al.*, "Stacking disorder in ice I," *Phys. Chem. Chem. Phys.* **17**, 60–76 (2015).
- ⁸²C. G. Salzmann *et al.*, "Ammonium fluoride as a hydrogen-disordering agent for ice," *J. Phys. Chem. C* **123**, 16486–16492 (2019).
- ⁸³J. Shephard *et al.*, "Doping-induced disappearance of ice II from water's phase diagram," *Nat. Phys.* **14**, 569–572 (2018).

- ⁸⁴A. L. Patterson and L. E. Alexander, "X-ray diffraction procedures for polycrystalline and amorphous materials," *J. Am. Chem. Soc.* **77**, 2030–2031 (1955).
- ⁸⁵B. Lee *et al.*, "Managing hydrogen bonding in the clathrate hydrate of the 1-pentanol guest molecule," *CrystEngComm* **23**, 4708–4716 (2021).
- ⁸⁶A. Wallqvist, "On the stability of type I gas hydrates in the presence of methanol," *J. Chem. Phys.* **96**, 5377–5382 (1992).
- ⁸⁷K. Koga, H. Tanaka, and K. Nakanishi, "On the stability of clathrate hydrates encaging polar guest molecules: Contrast in the hydrogen bonds of methylamine and methanol hydrates," *Mol. Simul.* **12**, 241–252 (1994).
- ⁸⁸K. Koga, H. Tanaka, and K. Nakanishi, "Stability of polar guest-encaging clathrate hydrates," *J. Chem. Phys.* **101**, 3127–3134 (1994).
- ⁸⁹Even though past experimental studies have shown that NH₄F-containing clathrate hydrates follow Vegard's Law of solid solution of a linear decrease of the cell parameters with increasing NH₄F-content, this behavior is not reflected in our simulations. (a) L. Vegard, "Die Konstitution der Mischkristalle und die Raumfüllung der Atome," *Z. Phys.* **5**, 17–26 (1921); (b) J. Kim *et al.*, "Incorporation of ammonium fluoride and methanol in carbon dioxide clathrate hydrates and their significance for hydrate-based gas separation," *Ind. Eng. Chem. Res.* **60**, 11267–11276 (2021); (c) K. Shin *et al.*, "Crystal engineering the clathrate hydrate lattice with NH₄F," *CrystEngComm* **16**, 7209–7217 (2014).
- ⁹⁰G. S. Hammond, "A correlation of reaction rates," *J. Am. Chem. Soc.* **77**, 334–338 (1955).
- ⁹¹K. Winkel *et al.*, "Structural transitions in amorphous H₂O and D₂O: The effect of temperature," *J. Phys.: Condens. Matter* **20**, 494212 (2008).
- ⁹²D. Blake, L. Allamandola, S. Sandford, D. Hudgins, and F. Freund, "Clathrate hydrate formation in amorphous cometary ice analogs in vacuo," *Science* **254**, 548–551 (1991).
- ⁹³R. L. Hudson and M. H. Moore, "Far-infrared investigations of a methanol clathrate hydrate: Implications for astronomical observations," *Astrophys. J.* **404**, L29–L32 (1993).
- ⁹⁴G. Natesco and A. Bar-Nun, "The effect of methanol clathrate-hydrate formation and other gas-trapping mechanisms on the structure and dynamics of cometary ices," *Icarus* **148**, 456–463 (2000).
- ⁹⁵S. Facq, F. Danède, and B. Chazallon, "Ethanol hydrates and solid solution formed by gas condensation: An in situ study by micro-Raman scattering and X-ray diffraction," *J. Phys. Chem. A* **114**, 10646–10654 (2010).